nature nanotechnology

Letter

https://doi.org/10.1038/s41565-022-01285-z

DNA double helix, a tiny electromotor

Received: 15 March 2022

Accepted: 4 November 2022

Published online: 23 December 2022



Check for updates

Christopher Maffeo 12, Lauren Quednau, James Wilson & Aleksei Aksimentiev

1,2,3

Flowing fluid past chiral objects has been used for centuries to power rotary motion in man-made machines. By contrast, rotary motion in nanoscale biological or chemical systems is produced by biasing Brownian motion through cyclic chemical reactions. Here we show that a chiral biological molecule, a DNA or RNA duplex rotates unidirectionally at billions of revolutions per minute when an electric field is applied along the duplex, with the rotation direction being determined by the chirality of the duplex. The rotation is found to be powered by the drag force of the electro-osmotic flow, realizing the operating principle of a macroscopic turbine at the nanoscale. The resulting torques are sufficient to power rotation of nanoscale beads and rods, offering an engineering principle for constructing nanoscale systems powered by electric field.

Although incremental miniaturization of a man-made machine is possible by simply reducing the size of its parts, radical miniaturization typically requires re-evaluation of the physical principles that govern the machine's operation¹. For example, in a conventional electromotor, an electric field is transformed into rotary motion by means of electromagnetic induction. However, rotary motion is already best produced at the submillimetre scale using electrostatic actuation². At the nanoscale, biological molecular motors operate with high precision and efficiency³ using a chemical reaction to bias direction of random displacement⁴. Some molecular motors, such as FoF1 ATP synthase⁵ and the bacterial flagellum motor⁶, are true electromotors, transforming the energy of a transmembrane electric potential into rotation⁷. Although the biased diffusion mechanism has been realized in purely synthetic molecular systems^{8,9}, none of those matched the precision and efficiency of a biological motor, which ultimately can be attributed to the latter having structures optimized by evolution.

The years of evolution that furnished DNA might have given us more than just the carrier of the genetic code. The programmable self-assembly of DNA molecules has emerged as a powerful tool for soft nanotechnology 10,11, enabling fabrication of a diverse range of systems¹²⁻¹⁵. Using the DNA hybridization reaction as fuel¹⁶, molecular motors have been constructed to walk¹⁷⁻²¹, roll²² or pivot²³ on a pre-defined track; to transport²⁴ and sort²⁵ molecular cargoes; and to undergo reversible conformational transitions²⁶. Aimed at reproducing biological function of molecular motors, multi-subunit concentric DNA origami structures were synthesized to undergo rotary diffusion, driven by stochastic forces^{27–29}. Unidirectional rotation of a self-assembled DNA arm was realized by coupling the arm's orientation to the direction of the fluid flow and alternating the flow direction in a cyclic pattern³⁰. Yet it has not escaped our notice that the screw shape of a DNA molecule could allow it to function as the simplest possible electromotor.

DNA duplex rotation in electric field

To investigate whether a single DNA duplex will rotate unidirectionally in an external electric field, we constructed an all-atom model of a 16 base pair (bp) DNA duplex submerged in 1 M KCl electrolyte solution (Fig. 1a). Using the all-atom molecular dynamics method, we simulated the behaviour of the duplex when an electric field was applied along its helical axis. The phosphorus atoms of the duplex were restricted to the surface of a cylinder such that the DNA duplex was free to rotate about its axis (see Methods for technical details).

With a 100 mV nm⁻¹ electric field directed along its helical axis, the DNA duplex was observed to rotate about its axis with the rotation vector pointing against the applied field (Fig. 1b and Supplementary Video 1). Similar unidirectional rotation was observed in a simulation performed using an alternative model of water (Extended Data Fig. 1a). Reversing the direction of the applied field reversed the direction of the DNA rotation. The DNA duplex was observed to rotate stochastically in the absence of the field.

Department of Physics, University of Illinois at Urbana-Champaign, Urbana, IL, USA. Beckman Institute for Advanced Science and Technology, University of Illinois at Urbana-Champaign, Urbana, IL, USA. 3Department of Bioengineering, University of Illinois at Urbana-Champaign, Urbana, IL, USA. ≥e-mail: aksiment@illinois.edu

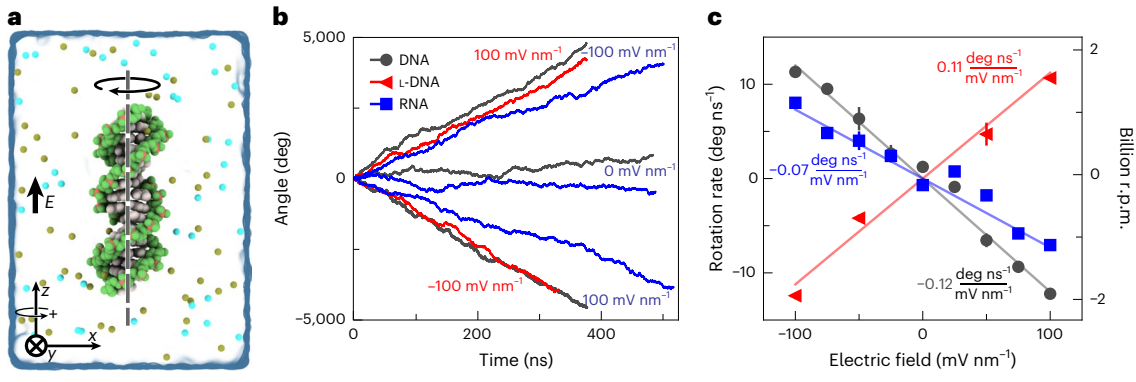


Fig. 1 | **Unidirectional rotation of DNA and RNA molecules in external electric field. a**, Simulation system containing a 16 bp DNA helix (light grey; green backbone) submerged in 1 M KCl electrolyte (semi-transparent molecular surface); only a fraction of ions is shown. An electric field E is applied parallel to the DNA helix. Phosphorus atoms of the DNA are harmonically restrained to the surface of a cylinder such that the DNA is free to rotate about its axis without drifting in the applied field. The circular arrow above the E-axis indicates a positive rotation direction. The arrow above the DNA indicates the direction of DNA rotation commensurate with the positive direction of the applied field.

b, Angular displacement of a DNA, L-DNA and RNA helix as a function of simulation time. The sign of displacement is defined in **a**. The electric field strength is annotated near each curve; the purple labels apply to both DNA and RNA. **c**, Average angular velocity of the DNA, L-DNA and RNA helices versus electric field strength. Each data point indicates an average value from a -400 ns molecular dynamics trajectory with error bars showing the standard error of the mean determined using 40 ns block-averaged data. Lines depict linear regression fits to the data. The right *y*-axis displays the rotational velocity in revolutions per minute (r.p.m.).

In a set of control computational experiments, we repeated our simulations using a 16 bp left-handed duplex constructed from L-DNA, the mirror image stereoisomer of biological DNA, finding the left-handed duplex to rotate with the same velocity as the canonical DNA duplex, but in the opposite direction (Fig. 1b and Supplementary Video 2). Finally, we repeated the simulation using a 16 bp A-form RNA duplex (Supplementary Video 3), finding the RNA to rotate in the same direction as the canonical B-DNA duplex, albeit with a reduced rate of rotation.

Repeating the simulations for several values of the electric field yielded the dependence of the average rotation rate on the electric field strength (Fig. 1c). Under a 100 mV nm $^{-1}$ electric field—a magnitude well within reach of nanopore translocation experiments 31 —the nucleic acid duplexes were found to spin at about 1 billion revolutions per minute, surpassing the rotation rate of the fastest known molecular rotors by several orders of magnitude.

Torque generation mechanism

To determine the torque imparted on the nucleic acid structures by the applied electric field, and the torque generation mechanism, we built all-atom systems in which a DNA or an RNA duplex was connected to itself across the periodic boundary of the simulation system, reproducing the case of an effectively infinite, straight duplex (Fig. 2a). Each phosphorus atom in the duplex was held to its initial coordinates using a harmonic restraining force (Fig. 2b and Extended Data Fig. 2a). Subject to external electric field, equilibrium displacement of the phosphorus atoms relative to their initial coordinates measured the effective force and torque experienced by the nucleic acid duplex.

Similar to our previous simulations of the effective force on a DNA duplex³², we find the effective force to be considerably reduced compared with the force expected from the nominal charge of the DNA molecule (Extended Data Fig. 2b). We previously showed that such an effective reduction of the DNA charge is caused, in part, by the drag of the electro-osmotic flow (Fig. 2c) that, in turn, is produced by the motion of counter-ions near the DNA surface³².

We determined the effective torque by multiplying the harmonic force restraining each phosphorus atom by the distance from the duplex axis to that atom (Fig. 2b). Averaging the torque values over all phosphorus atoms and the simulation trajectories yielded the dependence of the effective torque on the applied electric field (Fig. 2d), which

was insensitive to the water model used (Extended Data Fig. 1b). Under the same electric field, a DNA duplex was found to experience a greater torque per bp than an RNA duplex, which we attribute to the different shape of the molecules, with A-form RNA having a larger radius, smaller pitch (length of one turn) and a more solvent-accessible centre compared with B-form DNA. The torque, τ , and the angular velocity, ω , are related by $\omega = \mu \tau$, where μ is the rotational mobility (inverse of the rotational friction coefficient), which we determined by simulating forced rotation of the duplexes in the absence of applied electric field (Fig. 2e). The DNA duplex is found to have a slightly higher rotational mobility than an RNA duplex of the same nucleotide composition, in agreement with the mobility values extracted from the analysis of the rotational diffusion of the duplexes (Extended Data Fig. 3); thus, under the same electric field, an RNA duplex is expected to rotate more slowly than a DNA duplex as the former generates a lower effective torque and has a lower rotational mobility. We find that the rotation rate observed in our electric field simulations to be prescribed by the product of independently determined effective torque and rotational mobility (Extended Data Figs. 3 and 4).

To investigate the torque generation mechanism, we determined the magnitude of the fluid velocity directed along (Fig. 2c) – and tangential to (Fig. 2g)—the axis of the duplex as well as the local density of the fluid (Fig. 2f). Due to the grooves, the water density does not decrease all of the way to zero at radial distances shorter than those of the DNA backbone (~12 Å). Near and within the DNA duplex, the tangential component of the water flux has small yet statistically significant values, indicating that some of the water flux is redirected tangentially around the DNA in the directions expected from the helical geometry of the DNA duplex (Supplementary Videos 4 and 5). The momentum transfer caused by the redirection of the water flow imparts an effective tangential force, producing a non-zero net torque on the duplex (Fig. 2a). It should be stressed, however, that water here barely serves as a mediator of momentum transfer from cations because the latter move along, and tangentially to, the DNA duplex several times faster than water molecules do (Extended Data Fig. 5a-g). The ratio of the azimuthal mass fluxes separately carried by water and ions (Extended Data Fig. 5h) indicates that water accounts for ~80% of the azimuthal momentum that drives DNA rotation. Test simulations performed using a custom implicit water/explicit ions model show that both the DNA rotation rate and the effective torque would increase by a factor

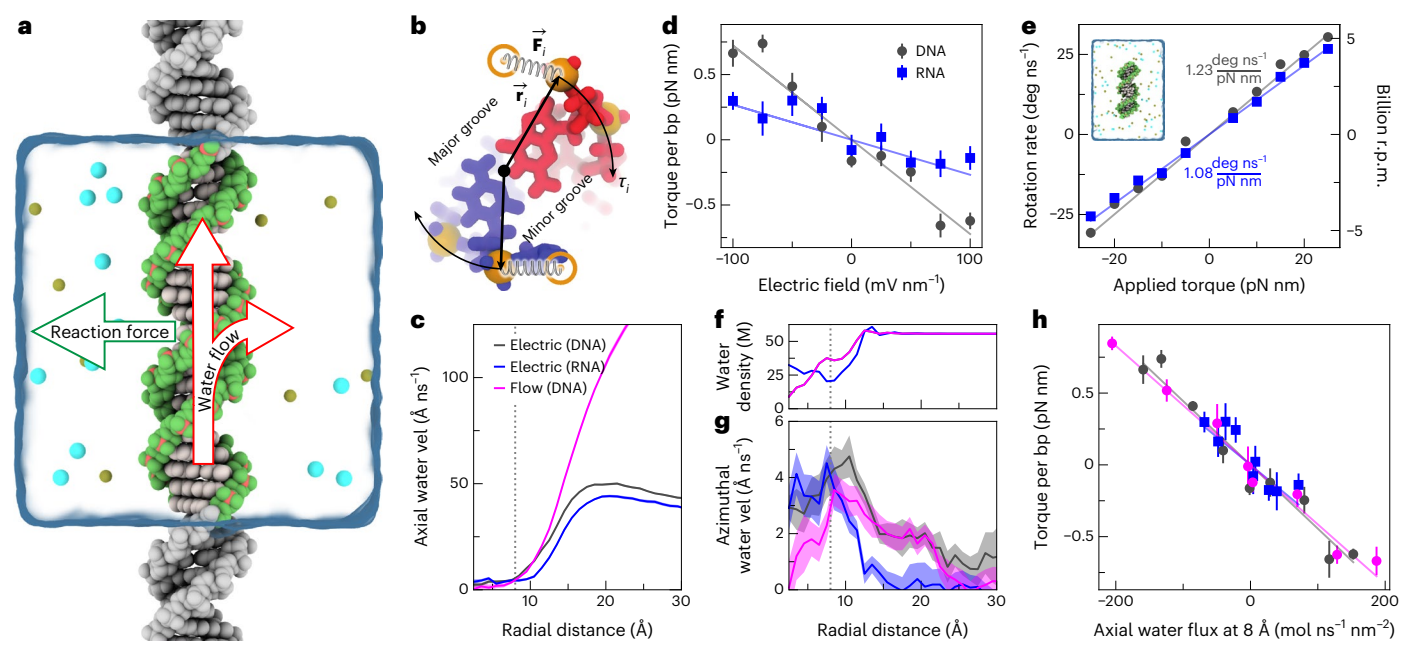


Fig. 2 | **Torque generation mechanism. a**, Schematics of the simulation system in which the DNA was made effectively infinite by connecting its stands over the periodic boundary. The arrows illustrate the torque generation mechanism: redirection of the water flow at the DNA surface. **b**, An illustration of a method used to measure or apply torque. A cross-section of the DNA construct is shown. **c**, Average water velocity along the duplex axis versus distance from the axis. Data were averaged over multiple trajectories at a ±50 mV nm⁻¹ electric field or a ±12.7 bar nm⁻¹ pressure gradient using 5 Å radial bins. Here and in **f** and **g**, a vertical dashed line indicates the location of a surface that is 8 Å away from the centre of DNA and RNA duplexes. **d**, Torque per bp exerted on DNA and RNA duplexes as a function of the electric field. Lines show linear fits to the data. Each data point indicates the average value from a -100 ns molecular dynamics trajectory; the error bars show the standard error of the mean computed using 20 ns block-averaged data. **e**, Rotation rate as a function of applied torque. Each data point indicates the average value from a 100–300 ns molecular dynamics

trajectory; the error bars show the standard error of the mean computed using 20 ns block-averaged data. The data were obtained using finite length (16 bp) DNA and RNA molecules (one such system is shown in the inset). The slope of the linear fit (lines) to the data is the rotational mobility of the duplexes. **f**, Density of water molecules versus distance from the duplex axis. For the DNA system, the electric field and solvent flow data overlap almost exactly. **g**, Average tangential water velocity versus radial distance from the central axis of the DNA or RNA duplex. Data were computed as described in **e**. The shaded regions depict the magnitude of the difference between data obtained at opposite directions of the electric field, whereas the solid lines depict the average over the two directions. **h**, Torque versus axial water velocity 8 Å away from the centre of DNA and RNA duplexes. Each data point indicates the average value from a 100–300 ns molecular dynamics trajectory; the error bars show the standard error of the mean computed using 20 ns block-averaged data.

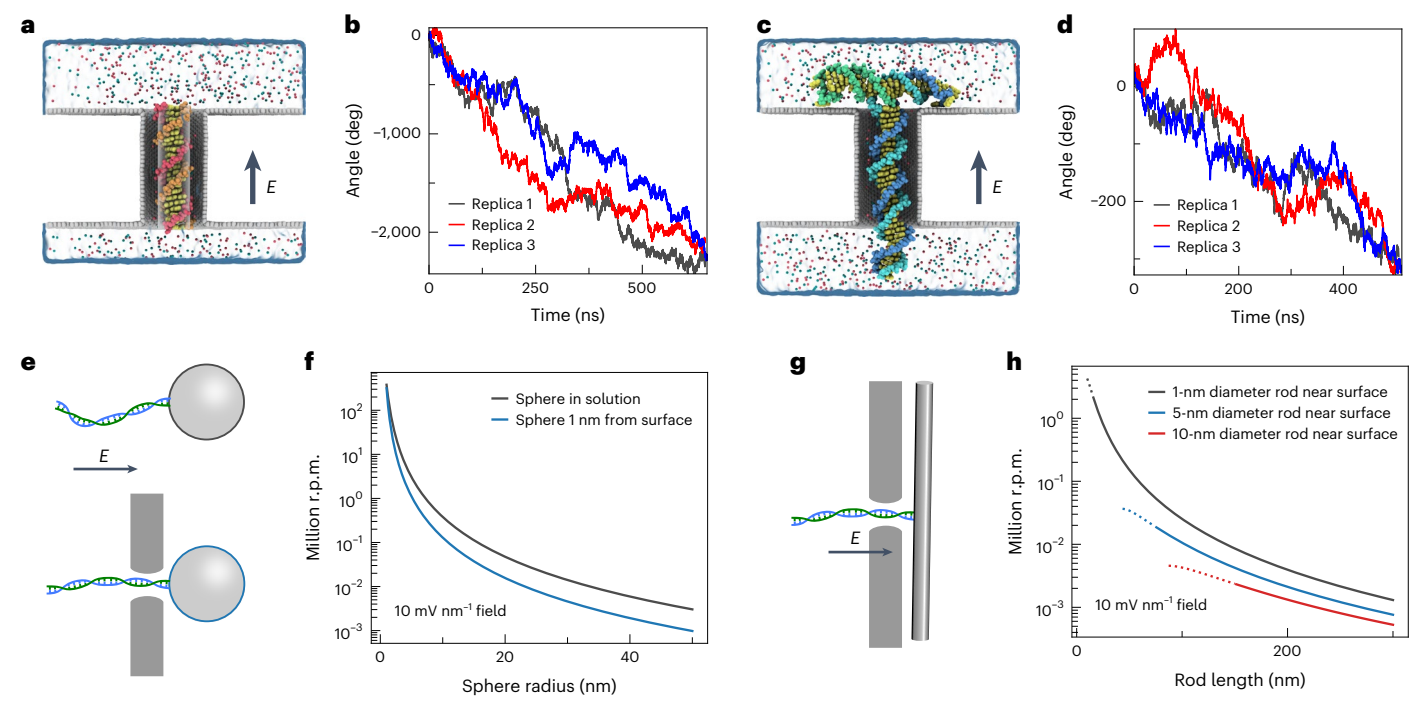
of five (Extended Data Fig. 6) if momentum dissipation through water could be avoided.

If the rotation of the duplexes in an electric field can be caused by the flow of the solvent, then it should be possible to observe such rotation in a system with a flow in the absence of the applied electric field. To test this hypothesis, along the DNA axis we applied a small force to every water molecule (Extended Data Fig. 7a), producing a steady-state water flow through the periodic DNA system (Fig. 2c). The flow, directed along the duplex axis, was observed to rotate DNA in the expected left-handed direction (Extended Data Fig. 7b and Supplementary Video 6). The rotation rate was seen to depend linearly on the hydrostatic pressure gradient (Extended Data Fig. 7c). Despite the net flux of solvent being much larger in the pressure-driven simulation than when induced by the electro-osmotic effect (Fig. 2c), the rotation rates in both cases are of similar magnitudes (compare Fig. 1c and Extended Data Fig. 7c), which we attribute to the similar variation of the flow profile near the surface of the DNA duplex. In fact, we find the measured torques to fall on the same master curve when plotted versus the magnitude of axial water flux measured 8 Å away from the centre of the nucleic acid duplex (Fig. 2h).

Nanopore-powered rotation

A practical approach to using DNA for torque generation would be to thread a DNA molecule through a nanopore in a thin membrane, arresting the DNA translocation through the nanopore by using a load that is too large to pass through it. We demonstrate this possibility by first simulating rotation of a DNA fragment confined within a carbon nanopore (Fig. 3a). Under a 197 mV bias, the DNA was observed to rotate at an average rate of 3.2 degrees per nanosecond (Fig. 3a and Supplementary Video 7) as water moved through the nanopore at an average speed of 0.42 nm ns⁻¹ driven by an ionic current of 1.1 nA. Knowing the rotational mobility of a DNA duplex (Fig. 2e), we estimate the effective torque applied to the DNA in these simulations at 3.4 pN nm. Neglecting dissipation due to the thermostat, we estimate the power input to be -200 pW from the product of current and voltage. From the ratio of the input power to the mechanical work done to rotate the helix by 28 million revolutions in 1 s, we estimate an energy conversion efficiency of -0.1%.

To elucidate the effect of friction between the load-arresting DNA translocation and the membrane surface, we simulated spontaneous diffusion of a DNA duplex pressed towards the graphene layer by an external force (Supplementary Video 8). Without loosening the contact with graphene, the duplex was seen to undergo pronounced translational and rotation diffusion on a time-scale of 150 ns (Extended Data Fig. 8). Encouraged by this result, we constructed a DNA T-bar comprising a 30 bp duplex connected orthogonally to a 20 bp dumbbell (Fig. 3c and Extended Data Fig. 9). Subject to a 394 mV bias, the T-bar was observed to rotate in the carbon nanopore with the rate of 0.58 degrees per nanosecond in the absence of any external restrains applied to the DNA (Fig. 3d and Supplementary Video 9). Note that increasing the



 $\label{eq:fig.3} IDNA-powered rotation of hydrodynamic loads. a, Cut-away view of a simulation system consisting of a 21 bp DNA duplex placed co-axially to a carbon nanopore comprising a 3.6 nm diameter carbon nanotube fused to two rigid graphene layers, separated by 6.5 nm. The phosphorus atoms of the duplex are restricted to the surface of a cylinder within the nanopore using restraints identical to those employed in the simulations depicted in Fig. 1. The nanopore surface was negatively charged at <math display="inline">-0.058$ e nm $^{-2}$ to increase the electro-osmotic flow, where e is the charge of a proton. b, Rotation angle of the DNA duplex as a function of simulation time for three replica simulations under a 197 mV transmembrane potential. c, Simulation system consisting of a carbon nanopore and a T-bar DNA construct. d, Rotation angle of the T-bar DNA construct as a function of simulation time in three replica simulations under a 394 mV transmembrane potential. e, Schematic of a model system where a DNA molecule

is tethered, with both of its ends, to a spherical nanoparticle and is threaded through a nanopore in a membrane, with the latter being either far from (top, membrane not depicted) or near to (bottom) the nanoparticle. **f**, Theoretical dependence of the rotation rate of a spherical nanoparticle on the nanoparticle's radius under a 1 pN nm torque on the DNA. Here, and in **h**, the rotation rate was computed as the ratio of the applied torque and the friction coefficient of the load, neglecting the drag from the rest of the DNA molecules due to its relatively small value (Extended Data Fig. 10). **g**, A variant of a model system shown in **e** but with the DNA molecule threaded through a nanopore and tethered to a rod-like nanoparticle. **h**, Theoretical dependence of the rotation rate on the rod length for the system depicted in **g**. The dotted lines indicate the regime in which the length is comparable to the rod diameter, invalidating the approximations used to derive the expression for the rotational diffusion coefficient of a cylinder near a surface.

magnitude of the nanopore electro-osmotic flow both reduces the effective force pulling the DNA through and increases the effective torque, which makes smooth and negatively charged nanopores^{33–35} ideal for torque generation using DNA.

Armed with theoretical expressions for the hydrodynamic drag of spherical and rod-like particles (see Methods and Extended Data Fig. 10) and assuming a 1 pN nm torque on the duplex, we determined the steady-state rotational velocity of larger loads attached to the end of a DNA molecule (Fig. 3e–h). We find the average rotation rate of the spherical particle to decrease from millions to thousands of revolutions per minute as the particle radius increases from 10 to 40 nm (Fig. 3f). Similar calculations for a rod-like load (Fig. 3g) yield rotation rates that decrease with the length of the rod and are in the range of tens of thousands of revolutions per minute for 200-nm-long rod (Fig. 3h). As the torque on the DNA is caused by the solvent flow, similar magnitude rotations can be expected when the flow is generated using a salinity gradient 36.

Our calculations suggest that a DNA molecule is subject to considerable torques in typical nanopore translocation experiments. Given that torsion propagates much faster along a DNA molecule than tension, with the latter being defined by the 3D configuration of the molecule³⁷, the torque applied to the DNA within the nanopore could, potentially, induce the formation of plectonemes in the DNA structure upstream from the nanopore. The passage of plectonemes through a nanopore would register as a transient threefold increase in the depth

of the blockade current, a current blockade signature similar to that produced by the passage of a DNA knot³⁸. Experimentally, the rotation of DNA in a nanopore could be detected by attaching the DNA to a stiff fluorescently labelled rod, to an asymmetric plasmonic nanoparticle or to a magnetic bead.

Conclusion

In summary, we have shown that the very chiral shape of a DNA duplex is sufficient to generate a rotary motion when solvent moves past its surface. Such fluid motion can be conveniently produced by applying electric field along the DNA helix, utilizing the electro-kinetic effect. The torques generated by the effect are sufficiently large to power rotation of 10-200 nm scale loads with rates on par or exceeding those of biological molecular motors. By contrast to molecular motors, however, the torque generation mechanism in the DNA turbine closely resembles that for a macroscopic turbine, suggesting that other macroscopic machines that rely on fluid flow for their operation can be scaled down to the nanoscale.

Online content

Any methods, additional references, Nature Portfolio reporting summaries, source data, extended data, supplementary information, acknowledgements, peer review information; details of author contributions and competing interests; and statements of data and code availability are available at https://doi.org/10.1038/s41565-022-01285-z.

References

- Pelesko, J. A. & Bernstein, D. H. Modeling MEMS and NEMS (CRC, 2002).
- Tsoukalas, K., Vosoughi Lahijani, B. & Stobbe, S. Impact of transduction scaling laws on nanoelectromechanical systems. *Phys. Rev. Lett.* 124, 223902 (2020).
- Bustamante, C., Keller, D. & Oster, G. The physics of molecular motors. Acc. Chem. Res. 34, 412–420 (2001).
- Julicher, F., Ajdari, A. & Prost, J. Modeling molecular motors. Rev. Mod. Phys. 69, 1269–1281 (1997).
- Boyer, P. D. The ATP synthase—a splendid molecular machine. Annu. Rev. Biochem. 66, 717–749 (1997).
- Deme, J. C. et al. Structures of the stator complex that drives rotation of the bacterial flagellum. Nat. Microbiol. 5, 1553–1564 (2020).
- Junge, W., Lill, H. & Engelbrecht, S. ATP synthase: an electrochemical transducer with rotatory mechanics. *Trends Biochem. Sci.* 22, 420–423 (1997).
- Hernández, J. V., Kay, E. R. & Leigh, D. A. A reversible synthetic rotary molecular motor. Science 306, 1532–1537 (2004).
- 9. Roke, D., Wezenberg, S. J. & Feringa, B. L. Molecular rotary motors: Unidirectional motion around double bonds. *Proc. Natl Acad. Sci. USA* **115**, 9423–9431 (2018).
- Seeman, N. C. & Sleiman, H. F. DNA nanotechnology. *Nat. Rev. Mater.* 3, 17068 (2017).
- 11. Rothemund, P. W. K. Folding DNA to create nanoscale shapes and patterns. *Nature* **440**, 297–302 (2006).
- Gu, H., Chao, J., Xiao, S.-J. J. & Seeman, N. C. A proximity-based programmable DNA nanoscale assembly line. *Nature* 465, 202–205 (2010).
- Modi, S. et al. A DNA nanomachine that maps spatial and temporal pH changes inside living cells. Nat. Nanotechnol. 4, 325–330 (2009).
- Marras, A. E., Zhou, L., Su, H.-J. & Castro, C. E. Programmable motion of DNA origami mechanisms. *Proc. Natl Acad. Sci. USA* 112, 713–718 (2015).
- Kosuri, P., Altheimer, B. D., Dai, M., Yin, P. & Zhuang, X. Rotation tracking of genome-processing enzymes using DNA origami rotors. *Nature* 572, 136–140 (2019).
- Yurke, B., Turberfield, A. J., Mills, A. P., Simmel, F. C. & Neumann, J. L. A DNA-fuelled molecular machine made of DNA. *Nature* 406, 605–608 (2000).
- Shin, J.-S. & Pierce, N. A. A synthetic DNA walker for molecular transport. J. Am. Chem. Soc. 126, 10834–10835 (2004).
- Green, S., Bath, J. & Turberfield, A. Coordinated chemomechanical cycles: a mechanism for autonomous molecular motion. *Phys. Rev. Lett.* 101, 238101 (2008).
- 19. Omabegho, T., Sha, R. & Seeman, N. C. A bipedal DNA Brownian motor with coordinated legs. *Science* **324**, 67–71 (2009).
- Lund, K. et al. Molecular robots guided by prescriptive landscapes. Nature 465, 206–210 (2010).
- Khara, D. C. et al. DNA bipedal motor walking dynamics: an experimental and theoretical study of the dependency on step size. Nucl. Acids Res. 46, 1553–1561 (2017).

- Bazrafshan, A. et al. Tunable DNA origami motors translocate ballistically over µm distances at nm/s speeds. *Angew. Chem. Int. Ed.* 59, 9514–9521 (2020).
- Tomaru, T., Suzuki, Y., Kawamata, I., Shin-ichiro, M. N. & Murata, S. Stepping operation of rotary DNA origami device. *Chem. Commun.* 53, 7716–7719 (2017).
- 24. Wang, Z.-G., Elbaz, J. & Willner, I. A dynamically programmed DNA transporter. *Angew. Chem. Int. Ed.* **51**, 4322–4326 (2012).
- Thubagere, A. J. et al. A cargo-sorting DNA robot. Science 357, eaan6558 (2017).
- 26. Kuzyk, A. et al. Reconfigurable 3D plasmonic metamolecules. *Nat. Mater.* **13**, 862–866 (2014).
- 27. Ketterer, P., Willner, E. M. & Dietz, H. Nanoscale rotary apparatus formed from tight-fitting 3D DNA components. *Sci. Adv.* **2**, e1501209 (2016).
- 28. Ahmadi, Y. et al. The brownian and flow-driven rotational dynamics of a multicomponent DNA origami-based rotor. *Small* **16**, 2001855 (2020).
- Bertosin, E. et al. A nanoscale reciprocating rotary mechanism with coordinated mobility control. *Nat. Commun.* 12, 7138 (2021).
- Kopperger, E. et al. A self-assembled nanoscale robotic arm controlled by electric fields. Science 359, 296–301 (2018).
- 31. Tripathi, P. et al. Electrical unfolding of cytochrome c during translocation through a nanopore constriction. *Proc. Natl Acad. Sci. USA* **118**, e2016262118 (2021).
- Luan, B. & Aksimentiev, A. Electro-osmotic screening of the DNA charge in a nanopore. *Phys. Rev. E* 78, 021912 (2008).
- 33. Holt, J. K. et al. Fast mass transport through sub-2-nanometer carbon nanotubes. *Science* **312**, 1034–1037 (2006).
- Siria, A. et al. Giant osmotic energy conversion measured in a single transmembrane boron nitride nanotube. *Nature* 494, 455–458 (2013).
- 35. Secchi, E. et al. Massive radius-dependent flow slippage in carbon nanotubes. *Nature* **537**, 210–213 (2016).
- 36. Marbach, S. & Bocquet, L. Osmosis, from molecular insights to large-scale applications. *Chem. Soc. Rev.* **48**, 3102–3144 (2019).
- 37. Chen, K. et al. Dynamics of driven polymer transport through a nanopore. *Nat. Phys.* **17**, 1043–1049 (2021).
- 38. Plesa, C. et al. Direct observation of DNA knots using a solid-state nanopore. *Nat. Nanotechnol.* **11**, 1093–1097 (2016).

Publisher's note Springer Nature remains neutral with regard to jurisdictional claims in published maps and institutional affiliations.

Springer Nature or its licensor (e.g. a society or other partner) holds exclusive rights to this article under a publishing agreement with the author(s) or other rightsholder(s); author self-archiving of the accepted manuscript version of this article is solely governed by the terms of such publishing agreement and applicable law.

© The Author(s), under exclusive licence to Springer Nature Limited 2022

Methods

All-atom molecular dynamics simulations

General simulation protocol. Unless specified otherwise, all-atom molecular dynamics simulations were performed using the NAMD program 39 , and CHARMM36 parameters were used for DNA, water and ions 40,41 , with CUFIX 42 corrections, periodic boundary conditions and the TIP3P model of water 43 . The long-range electrostatic interactions were computed using the particle-mesh Ewald scheme over a 1-Å-spaced grid 44 . Van der Waals and short-range electrostatic forces were evaluated using the 10–12 Å smooth cut-off scheme. The integration time step was 2 fs, and the full electrostatics were calculated every three time steps.

Assembly of the nucleic acid duplex systems. Five all-atom models of nucleic acid systems were constructed using the nucleic acid builder⁴⁵. The first two models were built from either DNA or RNA nucleotides according to the (AT)₈ sequence. A custom conversion script was used to transform the coordinates of the 16 bp DNA fragment to produce a complementary L-DNA model. The two-turn periodic DNA and RNA constructs were built from the d(ACTG)₅dA (10.5 bp per turn) and (ACUG)₅AC (11 bp per turn) sequences, respectively. The strands of the periodic constructs were connected to themselves over the periodic boundaries using the LKNA patch. Water and ions were added to each system using the 'Solvate' and 'Autoionize' plugins of VMD⁴⁶, producing a volume of 1 M KCl solution that submerges nucleic acids. Each system was minimized for 1,000 steps while harmonically restraining each phosphorus atom to its initial coordinates using a 0.1 kcal mol⁻¹ Å⁻² spring constant. The systems were equilibrated for 15 ns under the same position restrains using the Nosé-Hoover Langevin piston, with 295 K and 1 atm targets for temperature and pressure, respectively. For non-periodic systems, the dimensions orthogonal to the DNA axis were kept fixed during equilibration whereas the dimension parallel to DNA axis (z-axis) was allowed to fluctuate to meet the pressure target. For periodic systems, the orthogonal dimensions could fluctuate independently from the parallel dimension in such a way that the aspect ratio of the orthogonal plane was preserved. The Langevin damping coefficient was 0.1 ps⁻¹.

Simulations of nucleic acid duplex under applied electric field. All applied electric field simulations were performed in a constant-number-of-atoms, -volume and -temperature (*NVT*) ensemble. The system's dimensions were set to the average values from the equilibration. A custom TclForces script was used to harmonically hold each phosphorus atom in DNA or RNA to a cylindrical surface (9.4 Å radius; 0.1 kcal mol⁻¹ Å⁻² spring constant)⁴⁷. The restraints allow the DNA and RNA molecules to rotate freely about their axes, but restrict them from moving off of a central axis. The phosphorus atoms were also restrained (with the same spring constants) to their idealized positions along the *z*-axis to prevent axial translation of the duplex in external electric field. To prevent fraying, the non-hydrogen atoms forming the terminal base pairs were reinforced (2.9 Å rest length; 4 kcal mol⁻¹ Å⁻² spring constant) using the extrabonds feature of NAMD.

Simulations under fluid flow. The simulations of nucleic acid constructs under a fluid flow were performed using the same protocols as in our applied electric field simulations, except, instead of an electric field, a small, constant force was applied to each water molecule parallel to the axis of the DNA molecule, generating a pressure differential of P = Nf/A, where f is the force applied to each of N water molecules in the system and A is the area of the system within the plane orthogonal to the direction of the applied force⁴⁸. The pressure gradient was then computed by dividing the pressure by the length of the system. The resulting flow velocity was determined by the force magnitude, which had a value between 20 to 300 fN for the simulations described in this work.

Effective torque measurements. To measure the force and torque, the simulations were performed exactly as described above, except that periodic systems were used, no cylinder restraints were used, and the phosphorus atoms of the duplex were harmonically restrained to their idealized positions (0.1 kcal mol $^{-1}$ Å $^{-2}$ spring constant) to prevent rotation. The instantaneous coordinates of the simulation system (frames) were written every 120 steps. The torque was calculated at each frame as the sum of the individual torques on the phosphorus atoms $\tau = \sum \left(\vec{\mathbf{F}}_i \times \vec{\mathbf{r}}_i\right) \cdot \mathbf{z}$ where $\vec{\mathbf{r}}_i$ is the vector from the geometric centre

of the phosphorus atoms to the *i*th phosphorus atom, \vec{F}_i is the restraining force and z is the unit vector along the DNA axis. The forces and torques were determined by post-processing the simulation trajectories using a custom script and were averaged over all frames. Finally, for simulations in which a torque was applied to the duplex to cause a rotation, the cylinder restraint TclForces script was modified to additionally apply a constant torque to each phosphorus atom.

Simulations using the TIP4P-D water model. The psfgen utility of NAMD2 was used to convert all water molecules of the infinite DNA simulation system (Fig. 2a) into the TIP4P-D⁴⁹ water model. All subsequent simulations of the TIP4P-D system followed the same protocols as our simulations of the TIP3P systems described above. Briefly, the system was equilibrated with the Nosé-Hoover Langevin Piston barostat for 96 ns. During equilibration, the cell-basis vector along the DNA axis was allowed to fluctuate independently from the other axes. Either a 10 or 100 mV nm⁻¹ electric field was then applied along the axis of the DNA while custom restraints were applied to the DNA duplex. In one simulation, the DNA phosphorus atoms were harmonically restricted to the surface of a cylinder (9.4 Å radius; 0.1 kcal mol⁻¹ Å⁻² spring constant), allowing rotation of the duplex while the centre of mass was restrained along the helical axis. In another simulation, the DNA phosphorus atoms were individually harmonically restrained (0.1 kcal mol⁻¹ Å⁻² spring constant) so that no rotation was possible. The displacement of the atoms from their restraint positions was used to compute the torque. The CUFIX⁴² corrections were adopted, although they have not been thoroughly validated for usage with the TIP4P-D water model.

Simulations of DNA diffusion along a graphene surface. The simulation systems comprised a 38 bp dsDNA placed on top of a hexagonal patch of a single layer of carbon atoms solvated by 1 M KCl electrolyte. The carbon layer patch was constructed using the Inorganic Builder plugin of VMD⁵⁰ and had a circumscribed radius of 14.7 nm. The volume occupied by the KCl electrolyte measured 6 nm along the axis orthogonal to the graphene plane. The system was simulated under hexagonal prism periodic boundary conditions. Parameters for the graphene atoms were adopted from ref. 51. During the simulations, the graphene atoms were harmonically restrained about their initial coordinates $(k_{\text{spring}} = 1.0 \,\text{kcal mol}^{-1})$. The system was equilibrated for 2.4 ns, with all non-hydrogen atoms of the DNA harmonically restrained $(k_{\text{spring}} = 1.0 \text{ kcal mol}^{-1})$ and the Nosé-Hoover Langevin Piston barostat set to 1 atm. The system was then simulated for 160 ns with the harmonic restrains on the DNA replaced by a constant 10 pN force (distributed among the phosphorus atoms) that pushed the DNA towards the graphene surface.

Simulations of DNA rotation in a carbon nanopore. The carbon nanopore system was constructed by first duplicating the single-layer graphene sheet described above and shifting one of them relative to the other by 6.5 nm normal to the planes of the sheets. A hexagonal pore with a circumscribed radius of ~1.8 nm was cut into both sheets. The dangling atoms of the sheets were connected to the ends of a 6.5-nm-long achiral carbon nanotube of a matching diameter. This procedure introduced six defects to the corners of each nanotube/graphene sheet junction: three carbon rings each containing seven

atoms and three carbon rings each containing nine atoms. The charge of each carbon nanotube atom was set to -0.0015 e, giving the nanopore surface a charge density of -0.058 e nm⁻².

A 21-bp-long DNA duplex was placed in the carbon nanopore, and the whole system was submerged in 1 M KCl electrolyte. No solvent molecules were placed in the toroidal volume surrounding the nanopore between the two graphene sheets. During all simulations, all atoms of the carbon nanopore (including the two carbon sheets) were harmonically restrained about their initial coordinates ($k_{\text{spring}} = 1.0 \text{ kcal mol}^{-1}$), except for the atoms within 4 Å of each nanotube/graphene sheet junction. To prevent possible melting of the DNA duplex, a harmonic bond restraint ($k_{\text{spring}} = 1.0 \text{ kcal mol}^{-1}$; 2.9 Å rest length) was placed between non-hydrogen purine N1 and pyrimidine N3 atoms of each base pair. The final system (Fig. 3a) was equilibrated for 2 ns, with all non-hydrogen atoms of the DNA harmonically restrained ($k_{\text{spring}} = 1.0 \text{ kcal mol}^{-1}$) to their initial coordinates and the Nosé-Hoover Langevin Piston barostat set to 1 atm. The DNA rotation simulations were performed in the NVT ensemble. A 197 mV bias of electric potential was induced across the membrane by applying a 15 mV nm⁻¹ uniform electric field normal to the graphene sheets⁵² while a custom TclForces script (see the "Simulations under applied electric field" section above for details) restrained the phosphorus atoms of the DNA to a cylindrical surface, preventing translation of the duplex. The ionic current through the nanopore was computed by summing up instantaneous displacements of all ions in the simulation system53.

Simulations of T-bar rotor in a carbon nanopore. The T-bar DNA motor was constructed using a custom mrDNA⁵⁴ script that placed a 20 bp DNA dumbbell terminated with 4 nt ssDNA caps (the bar of the T-bar motor) atop a 32 bp DNA helix (the stem of the T-bar rotor) that threaded the nanopore (Extended Data Fig. 9). A stacked three-way junction was employed to arrange the vector connecting the 3' and 5' ends of the stem duplex along the axis of the bar duplex to maximize torque transmission. In the construct, the junction between the stem and the bar was stabilized by only 5 bp. We note, however, that in experimental applications, such a junction could be made permanent by chemical cross-linking⁵⁵. The carbon nanopore had the same dimensions as above but all atoms were electrically neutral to reduce the electro-osmotic flow. As above, the system was solvated by a hexagonal prism volume of 1 M KCl electrolyte except for the region between the two graphene sheets. To prevent the atoms of the DNA backbone from sticking to the junction between the carbon nanopore and graphene. the non-bonded interactions between the backbone atoms ON3, ON6, CN7, CN8B, ON5 and P2 and the graphene carbon atoms were modified using the NBFIX approach, setting the depth of the potential well to −0.05 kcal mol⁻¹ and its minimum to 3.71 Å. The final system (Fig. 3c) was equilibrated for 2 ns with the barostat target pressure set to 1 atm. As above, a single harmonic bond restraint was added to each base pair of the stem duplex to prevent melting. Three replica simulations were then performed under a 394 mV bias in the NVT ensemble with no external restraints applied to the DNA.

Implicit solvent simulations of DNA rotation

In our implicit solvent simulations of DNA rotation, the DNA duplex was represented by a rigid body whereas potassium and chloride ions were represented as point particles. The rotational friction coefficient of the rigid-body about its axis was set to 1.23 degrees ns⁻¹ pN⁻¹ nm⁻¹, that is, the value extracted from the all-atom molecular dynamics simulations of DNA rotation (Fig. 2e). A bond spanning the periodic boundary connected dummy particles tethered to the two ends of the duplex and prevented rotation about axes orthogonal to the helical axis. The centre of mass of the duplex was harmonically restrained to prevent translation. The interactions between the rigid-body DNA and an ion were described via a three-dimensional potential of mean force that was previously obtained⁵⁶ for potassium and chloride ions using the

umbrella-sampling method⁵⁷. The three-dimensional potential map taken from ref. 56 was interpolated using a custom Python script to conform with the periodic DNA duplex geometry of the corresponding all-atom system (Fig. 2a). Extended Data Fig. 6a shows a 1 kcal mol⁻¹ isopotential surface of one such potential. The effective interaction potentials among and between the potassium and chloride ions were also taken from ref. 56. The friction coefficient of each ion was set to match the desired diffusivity of 203.7 Å² ns⁻¹ for potassium and 211.3 Å² ns⁻¹ for chloride, matching experimentally measured values⁵⁸. A 100 mV nm⁻¹ electric field was applied to the ions.

The effective torque applied to DNA in the implicit solvent simulations was measured by placing a harmonic dihedral angle potential (0.184 kcal mol $^{-1}$ degree $^{-2}$ spring constant) on a bead tethered to the edge of the duplex and three other beads with absolute coordinates that were harmonically restrained (100 kcal mol $^{-1}$ Å $^{-2}$ spring constant). The dihedral angle potential prevented rotation and directly reported the torque on the duplex produced by the motion of ions.

All implicit solvent simulations were performed using ARBD⁵⁶, an in-house-developed, GPU-accelerated Brownian and Langevin dynamics code for coarse-grained simulations. The Langevin dynamics integrator was used with a time-step set to 2 fs to facilitate direct comparison with all-atom molecular dynamics simulations.

Friction coefficients of rotating objects

The rotation rate calculation for a spherical particle located either away from, or in close proximity to, a membrane was performed using the following expressions for the hydrodynamic drag (friction coefficient) of the particle: $\xi_{\rm sph,\; away} = 8\pi\eta R^3$ and $\xi_{\rm sph,\; near} \approx 8\pi\eta R^3 \left(\zeta(3) - 3\left(\frac{n^2}{6} - 1\right)\left(\frac{d}{R} - 1\right)\right)^{59}$, respectively, where $\eta = 1.0016$ mPa s is the viscosity of water, R is the radius of the spherical particle, $\zeta(3) \approx 1.20206$ is Riemann's ξ function evaluated at 3, and d is the distance from the centre of the sphere to the membrane. As detailed in ref. 60, the above expressions were derived from steady-state solutions of the Navier-Stokes equation for a low-Reynolds number fluid with no-slip boundary conditions. In the case of a sphere in bulk solution, the expression was obtained using a perturbation expansion of the dimensionless parameter $\frac{R^2\omega}{v}$ about zero, where v is the kinematic viscosity. In the case in which the sphere rotates near a solid wall, an expansion is performed over h/R, where h is the distance of the wall from the surface of the sphere. The parameters involved in the expansions were less than one for all of the points considered.

The rotation rate calculations for a rod-like load were performed using the following expression for the friction coefficient of the rod: $\xi_{\rm rod} = \frac{8}{3}\pi\eta L^3/\left(\ln\left(\frac{L}{2R}\right) - 0.447\right)^{60}, \text{ where } L \text{ is half of the length and } R \text{ is the radius of the rod. As detailed in ref. 60, the above friction coefficient was derived from the low-Reynolds-number Navier–Stokes equation with no-slip boundary conditions approximately treating the rod as effectively infinite and writing its rotational friction coefficient per unit length in terms of the translational friction coefficient obtained from integration of the fluid stress tensor. In all cases, the rotation rate was computed as <math>\omega_{\rm particle} = \tau/\xi_{\rm particle}$ where τ was the effective torque on the duplex and $\xi_{\rm particle}$ was the friction coefficient of the particle.

Data availability

Simulation trajectories corresponding to the main text figures are available via https://doi.org/10.13012/B2IDB-6770800_V1. The datasets supporting the plots generated during the current study are attached. Any other data and simulation trajectories are available upon request.

Code availability

All simulation and analysis code are available on reasonable request. Source Data are provided with this paper.

References

- Phillips, J. C. et al. Scalable molecular dynamics on CPU and GPU architectures with NAMD. J. Chem. Phys. 153, 044130 (2020).
- Denning, E. J., Priyakumar, U. D., Nilsson, L. & MacKerell, A. D. Jr. Impact of 2-hydroxyl sampling on the conformational properties of RNA: update of the CHARMM all-atom additive force field for RNA. J. Comput. Chem. 32, 1929–1943 (2011).
- Hart, K. et al. Optimization of the CHARMM additive force field for DNA: improved treatment of the BI/BII conformational equilibrium. J. Chem. Theory Comput. 8, 348–362 (2012).
- Yoo, J. & Aksimentiev, A. Improved parametrization of Li, Na, K, and Mg ions for all-atom molecular dynamics simulations of nucleic acid systems. J. Phys. Chem. Lett. 3, 45–50 (2012).
- Jorgensen, W. L., Chandrasekhar, J., Madura, J. D., Impey, R. W. & Klein, M. L. Comparison of simple potential functions for simulating liquid water. J. Chem. Phys. 79, 926–935 (1983).
- Darden, T. A., York, D. & Pedersen, L. Particle mesh ewald: an N log(N) method for ewald sums in large systems. J. Chem. Phys. 98, 10089–10092 (1993).
- 45. Case, D. et al. Amber 12 Reference Manual (Amber, 2012).
- Humphrey, W., Dalke, A. & Schulten, K. VMD: visual molecular dynamics. J. Mol. Graph. 14, 33–38 (1996).
- Wilson, J. & Aksimentiev, A. Water-compression gating of nanopore transport. *Phys. Rev. Lett.* 120, 268101 (2018).
- 48. Zhu, F., Tajkhorshid, E. & Schulten, K. Pressure-induced water transport in membrane channels studied by molecular dynamics. *Biophys. J.* **83**, 154–160 (2002).
- Piana, S., Donchev, A. G., Robustelli, P. & Shaw, D. E. Water dispersion interactions strongly influence simulated structural properties of disordered protein states. J. Phys. Chem. B 119, 5113–5123 (2015).
- 50. Aksimentiev, A., Brunner, R., Cruz-Chu, E. R., Comer, J. & Schulten, K. Modeling transport through synthetic nanopores. *IEEE Nanotechnol. Mag.* **3**, 20–28 (2009).
- 51. Patra, N., Wang, B. & Král, P. Nanodroplet activated and guided folding of graphene nanostructures. *Nano Lett.* **9**, 3766–3771 (2009).
- Aksimentiev, A. & Schulten, K. Imaging a-hemolysin with molecular dynamics: ionic conductance, osmotic permeability and the electrostatic potential map. *Biophys. J.* 88, 3745–3761 (2005).
- Aksimentiev, A., Heng, J. B., Timp, G. & Schulten, K. Microscopic kinetics of DNA translocation through synthetic nanopores. *Biophys. J.* 87, 2086–2097 (2004).
- 54. Maffeo, C. & Aksimentiev, A. MrDNA: a multi-resolution model for predicting the structure and dynamics of DNA systems. *Nucleic Acids Res.* **48**, 5135–5146 (2020).
- Gerling, T., Kube, M., Kick, B. & Dietz, H. Sequence-programmable covalent bonding of designed DNA assemblies. Sci. Adv. 4, eaau1157 (2018).
- Comer, J. & Aksimentiev, A. Predicting the DNA sequence dependence of nanopore ion current using atomic-resolution brownian dynamics. J. Phys. Chem. C. 116, 3376–3393 (2012).

- Roux, B. The calculation of the potential of mean force using computer simulations. Comput. Phys. Commun. 91, 275–282 (1995).
- 58. Friedman, A. M. & Kennedy, J. W. The self-diffusion coefficients of potassium, cesium, iodide and chloride ions in aqueous solutions. *J. Am. Chem.* Soc. **77**, 4499–4501 (1955).
- 59. Liu, Q. & Prosperetti, A. Wall effects on a rotating sphere. J. Fluid Mech. 657, 1–21 (2010).
- 60. Pänke, O., Cherepanov, D. A., Gumbowski, K., Engelbrecht, S. & Junge, W. Viscoelastic dyanamics of actin filaments coupled to rotary F-ATPase: angular torque profile of the enzyme. *Biophys. J.* **81**, 1220–1233 (2001).

Acknowledgements

C.M. and A.A. acknowledge the illuminating discussions with X. Shi, C. Dekker and H. Dietz. A.A. acknowledges A. Noy for suggesting a carbon nanotube system and A. Smolyanitsky for suggesting an energy conversion calculation. This work was supported by the National Science Foundation grants DMR-1827346 and PHY-1430124 (A.A.). The supercomputer time was provided through XSEDE allocation grant MCA05S028 (A.A.) and the Leadership Resource Allocation MCB20012 on Frontera of the Texas Advanced Computing Centre (A.A.).

Author contributions

A.A. conceptualized and supervised the work, and performed project administration. A.A., C.M. and J.W. designed the methodology. C.M., L.Q. and J.W. performed the investigations and visualizations. A.A., C.M., L.Q. and J.W. acquired funding, and wrote the original draft, whereas A.A. and C.M. performed revisions.

Competing interests

The authors declare no competing interests.

Additional information

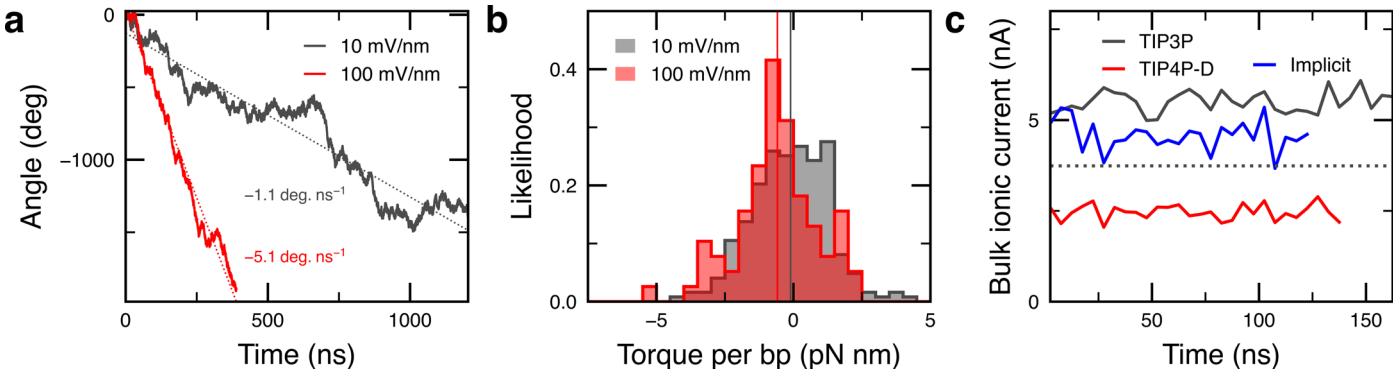
Extended data is available for this paper at https://doi.org/10.1038/s41565-022-01285-z.

Supplementary information The online version contains supplementary material available at https://doi.org/10.1038/s41565-022-01285-z.

Correspondence and requests for materials should be addressed to Aleksei Aksimentiev.

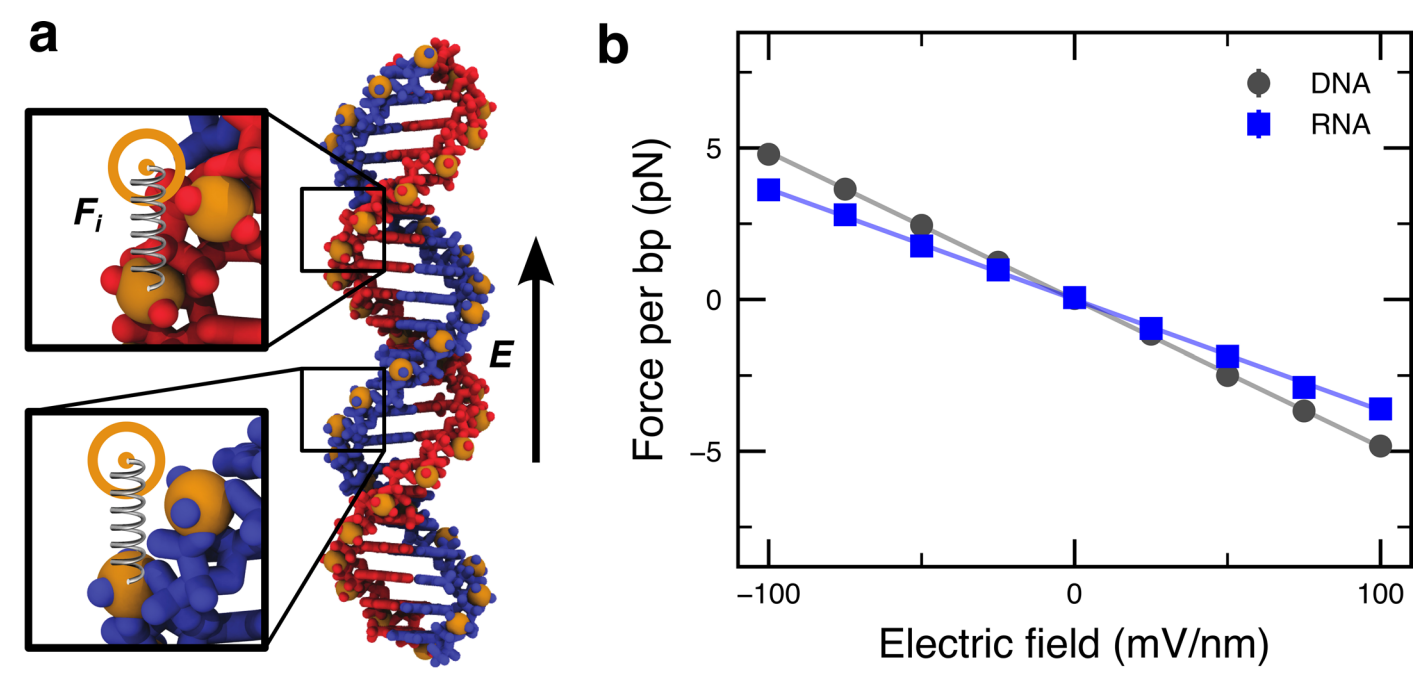
Peer review information *Nature Nanotechnology* thanks Derek Stein and the other, anonymous, reviewer(s) for their contribution to the peer review of this work.

Reprints and permissions information is available at www.nature.com/reprints.



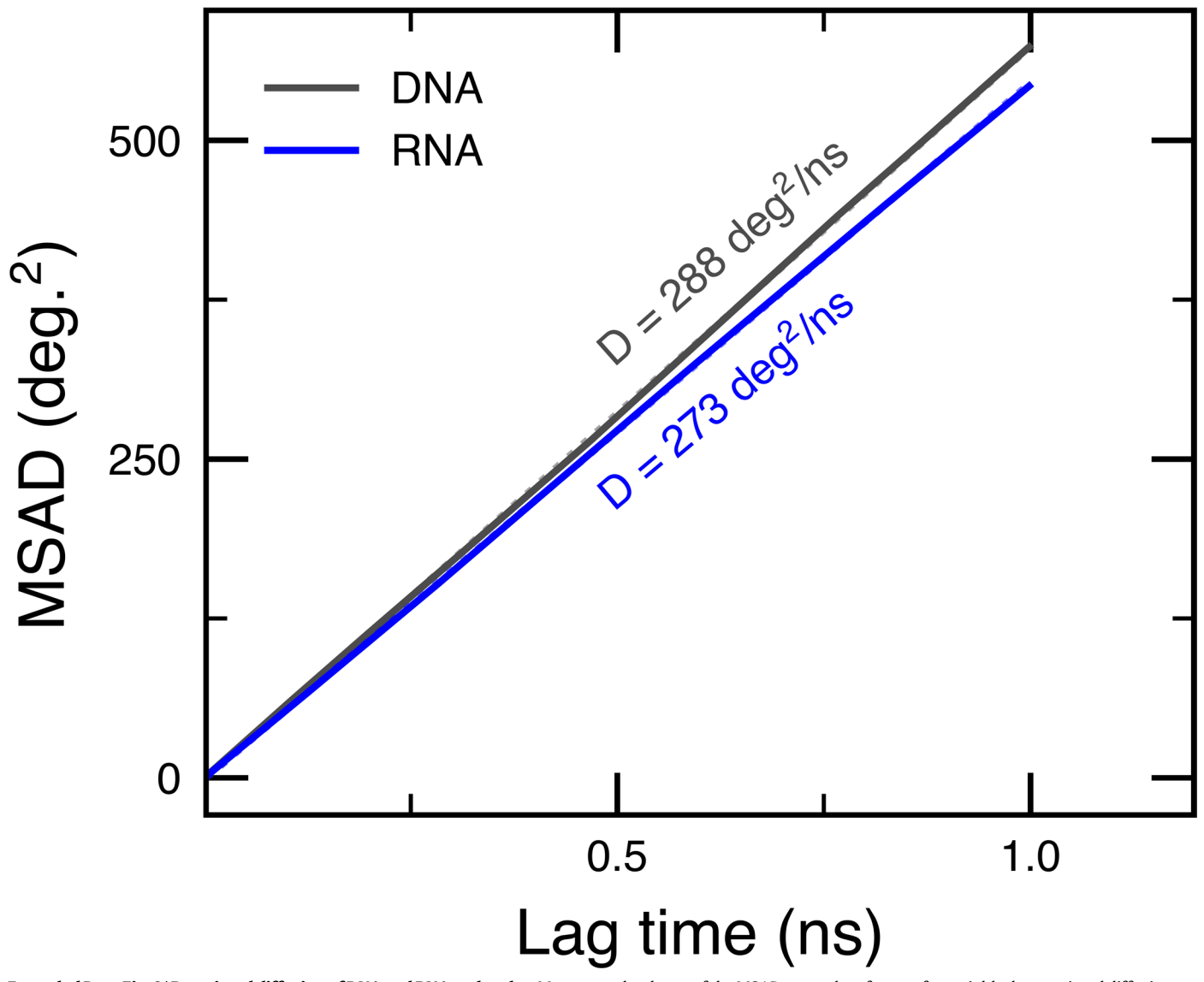
Extended Data Fig. 1| All-atom simulations of DNA rotation using the TIP4P-D water model. a, Rotation angle versus simulation time of a DNA duplex under 100 (red) and 10 (black) mV/nm electric field carried our using the TIP4P-D model of water. The simulation system was identical to the periodic TIP3P simulation system, Fig. 2a. The average rotation rate determined via a linear regression fit is -5.1 and -1.1 degrees/ns at 100 and 10 mV/nm, respectively. We attribute the non-linear scaling to a large statistical error of the 10 mV/nm simulation. For reference, the average rotation velocity observed in our TIP3P simulations under a 100 mV/nm field was -12.8 degrees/ns, Fig. 1c. b, Distribution of the effective torque values. The instantaneous torque values were sampled every 2.4 ps and averaged using 5 ns blocks. The vertical solid lines depict the mean values of the distributions: -0.74 and -0.11 pN nm for 100 and 10 mV/nm. For reference, the average magnitude of the effective torque measured using the TIP3P model of water is about 0.68 pN nm at electric field magnitude of

100 mV/nm, Fig. 2d. Thus, the torque values are insensitive to the water model used, indicating that the shear stress on DNA from the fluid does not depend on the fluid viscosity, as expected. c, lonic current through a cubic volume of 1 M KCl electrolyte, 5.8 nm on each side, under a 10 mV/nm electric field obtained using the TIP3P, TIP4P-D and out custom implicit solvent models, averaged over 5-ns blocks. For reference, the expected experimental ionic current value is plotted as a dashed line, computed using the experimental 11.0 S/m conductivity of 1 M KCl. The bulk conductivity values computed from the currents are 16.2, 7.2, and 13.5 S/m for the TIP3P, TIP4P-D and our custom implicit solvent models, respectively. The lower than experimental conductivity of the TIP4P-D electrolyte suggests that the model may systematically underestimate the electro-kinetic effects because of the lower than expected electrophoretic mobility of ions.



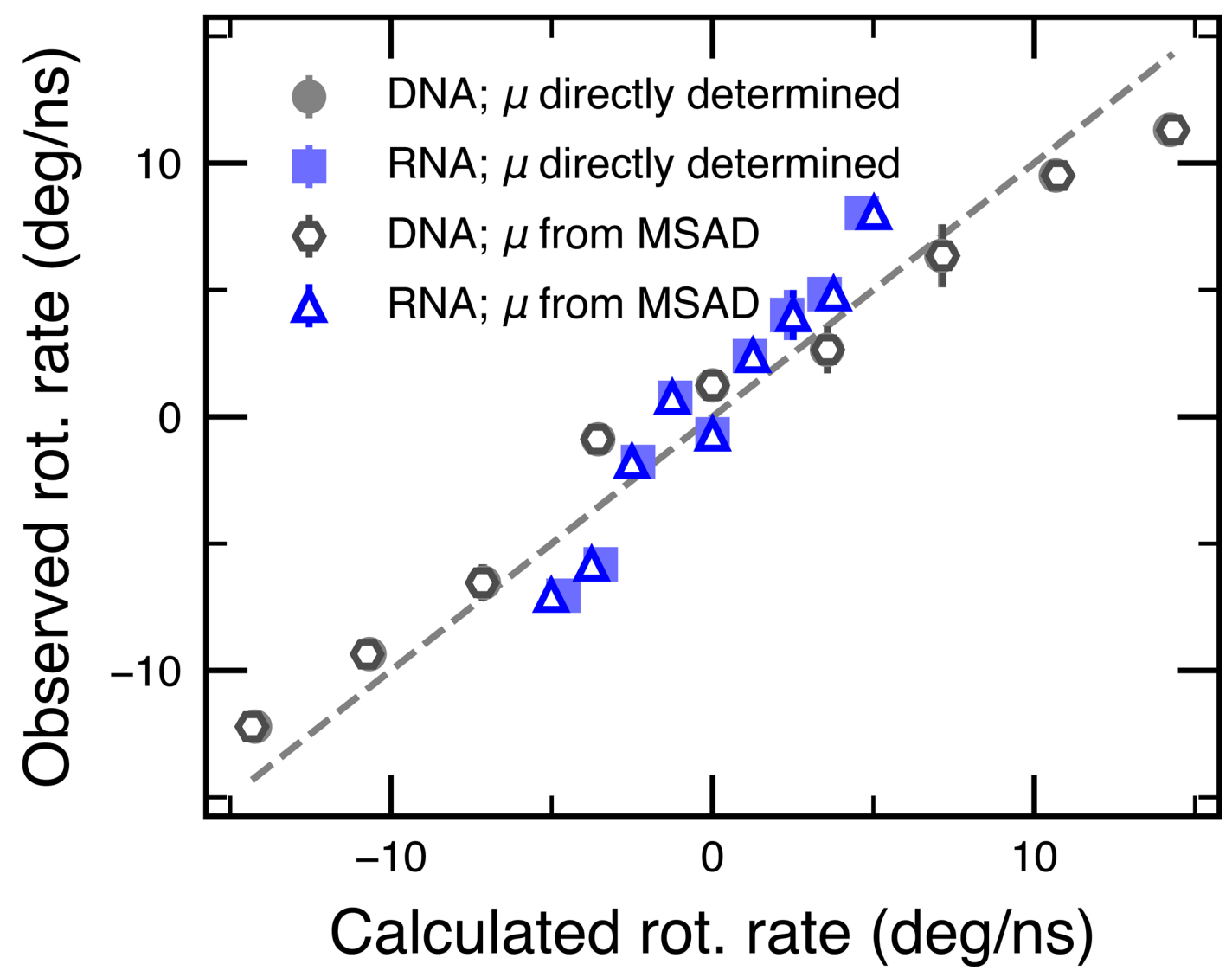
Extended Data Fig. 2 | Effective force of the electric field on DNA and RNA molecules. a, Simulation system containing a 21 bp DNA helix (blue and red strands; orange phosphorus atoms) submerged in a volume of 1 M KCl electrolyte (not shown). The insets schematically illustrate how the phosphorus atoms of the molecule are harmonically restrained to their initial coordinates. Equilibrium

displacement of the atoms from their initial coordinates along the nanopore axis multiplied by the spring constant of the harmonic restraint equals by magnitude the effective axial force experienced by the molecule. ${\bf b}$, Axial component of the module of the effective force, per base pair, on a DNA (black) or an RNA (blue) duplex as a function of the applied electric field.



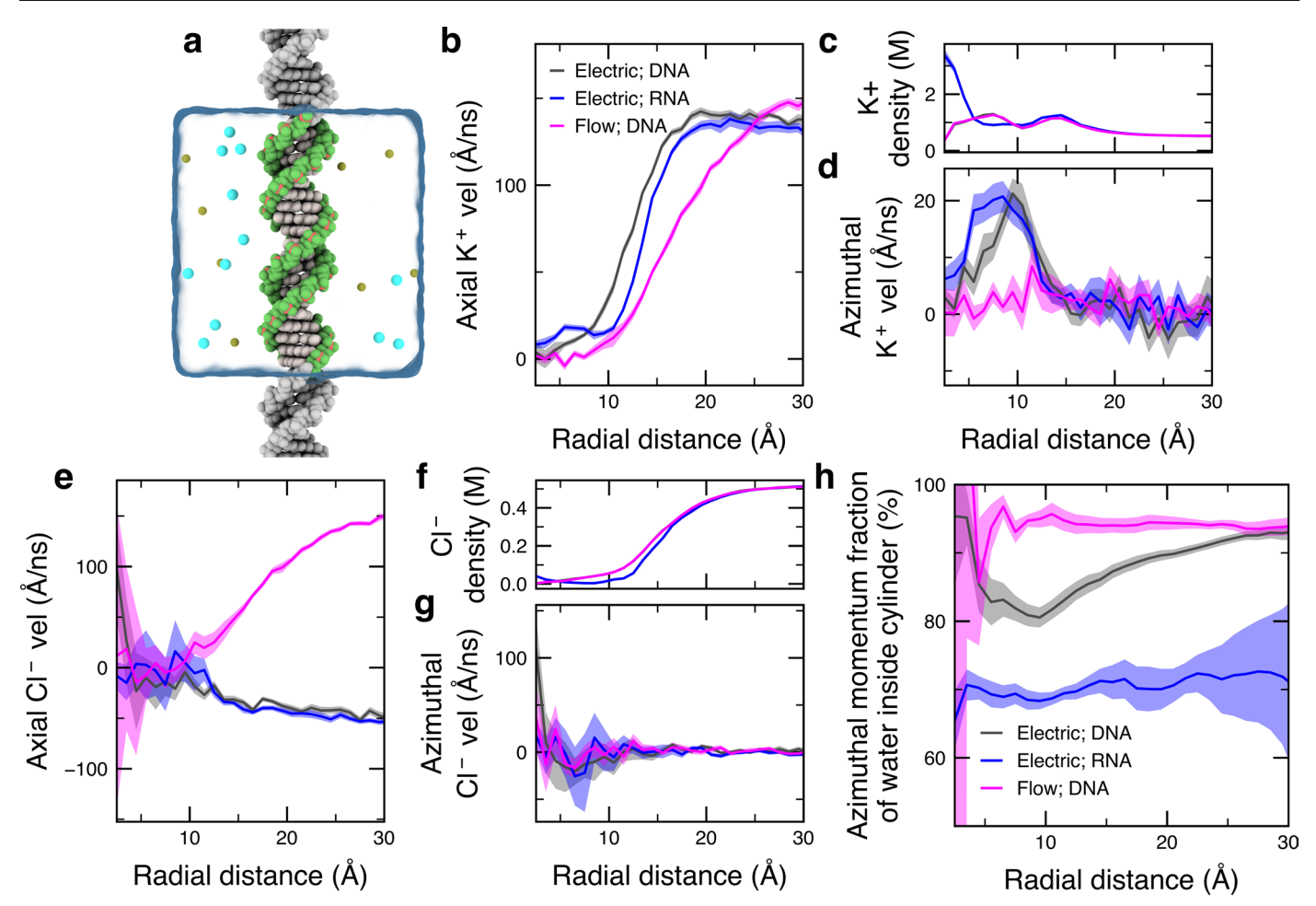
Extended Data Fig. 3 | **Rotational diffusion of DNA and RNA molecules.** Mean squared angular displacement (MSAD) of a 16-bp DNA (black) and a 16-bp RNA (blue) duplex is plotted versus the lag time. The MSAD values were determined from the analysis of the 500 ns angular displacement traces obtained under zero applied electric field conditions; the traces are shown in Fig. 1a. Dividing

the slopes of the MSAD curves by a factor of two yields the rotational diffusion constants, D, of DNA and RNA duplexes at 288 and 273 $\deg^2 ns^{-1}$, respectively. The corresponding rotational mobilities, $\mu = D/k_BT$, where k_BT is the thermal energy, are $\mu_{\rm DNA} = 1.24 \deg ns^{-1} pN^{-1} nm^{-1}$ and $\mu_{\rm RNA} = 1.17 \deg ns^{-1} pN^{-1} nm^{-1}$.



Extended Data Fig. 4 | Directly observed versus computed rate of rotation of a finite 16-bp duplex. The rate of rotation observed in the applied electric field simulations, Fig. 1c of the main text, is plotted versus the rotation rate calculated using two estimates of the angular mobility μ and the direct measurement of the torque under electric field, Fig. 2d. The torque per base pair was estimated from the applied field strength using the linear regression fit to the data, Fig. 2d. The rotation rate ω was calculated from the definition of mobility, $\mu = \omega/\tau$, where τ is

the torque on the duplex. Two strategies were used to determine the mobility: using the slope of the mean squared angular displacement as a function of lag time, Extended Data Fig. 3, and directly using the mobility determined from a linear regression fit to rotation rate due to a constant applied torque, Fig. 2e. We attribute slight deviations of the data from perfect agreement (dashed gray line) to a statistical error in determining the effective torque per base pair from Fig. 2d.



Extended Data Fig. 5 | Flow of ions around nucleic acid molecules.

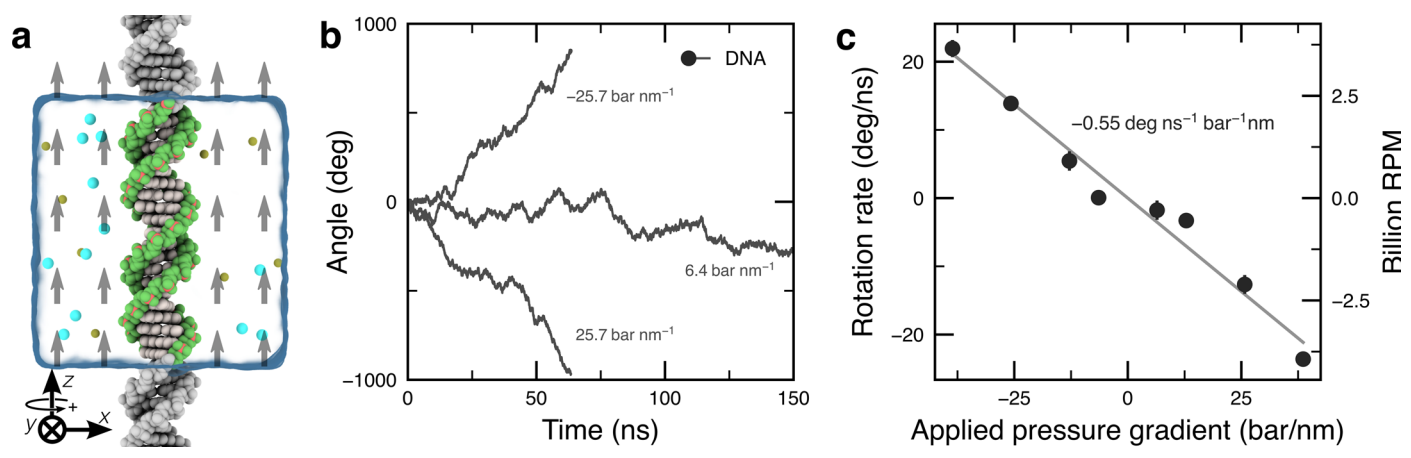
a, Schematic of the simulation system where the DNA was made effectively infinite by connecting its stands over the periodic boundary. A similar system was constructed for RNA. **b**, Average K^+ ion velocity along duplex axis versus distance from the axis. Data were averaged over multiple trajectories at ± 50 mV/nm electric field or ± 12.7 bar/nm pressure gradient using 5 Å radial bins. **c**, Density of water molecules versus distance from the duplex axis. For the DNA system, the electric field and solvent flow data overlap almost exactly. **d**, Average tangential velocity of a K^+ ion versus radial distance from the central axis of the DNA or RNA

duplex. Data were computed as described in panel b. $\mathbf{e}-\mathbf{g}$, Same as in panels b-d but for a Cl^ion. \mathbf{h} , Average tangential solvent momentum due to motion of water molecules within a cylindrical volume centred on the DNA or RNA duplex. At each radial value, the momentum of each solvent species was computed from the product of the average density, the average tangential velocity of the solvent species, the mass of that species and the radius. For all plots, the shaded regions depicts the magnitude of the difference between data obtained at opposite directions of the electric field; the solid lines depict the average over the two directions.

Extended Data Fig. 6 | Implicit solvent simulations of DNA rotation.

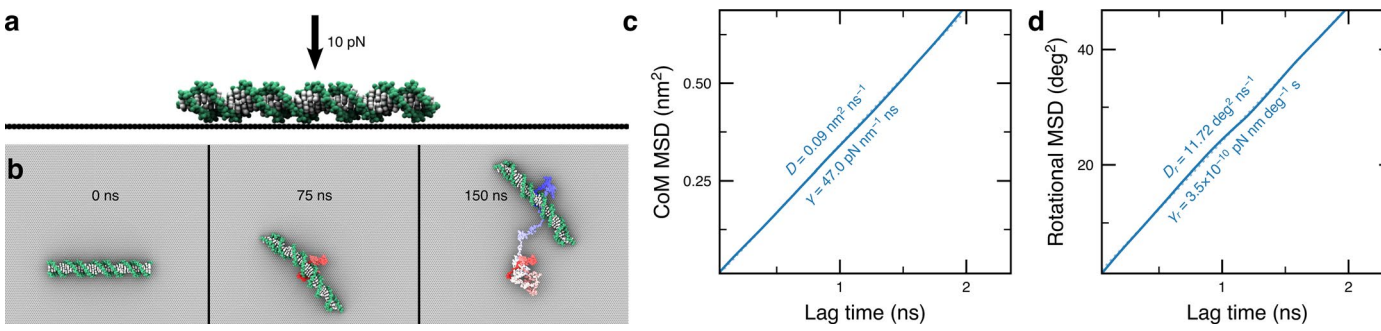
a, Simulation system consisting of a rigid body representation of a DNA duplex surrounded by point-like particles representing potassium (red) and chloride (teal) ions. Two grid-based potentials prescribe the interactions between the DNA duplex and the ions, a 1 kcal mol $^{-1}$ iso-surface for DNA–potassium potential is shown in grey. The DNA duplex is effectively infinite under the periodic boundary conditions. The centre of mass of the duplex is harmonically restrained to prevent translation. A 100 mV/nm electric field is applied to the ions.

 $\label{eq:bounds} \textbf{b}, Rotation angle as a function of simulations time for implicit solvent and all-atom simulations of DNA rotation under a 100 mV/nm electric field. The all-atom trace is from Fig. 1b. c, Average rotation rate versus electric field strength obtained from implicit solvent and all-atom simulations. The all-atom data are from Fig. 1c. d, Distributions of instantaneous torques, sampled every 2.4 ps and averaged over 5 ns blocks. A vertical solid line depicts the mean of each distribution. The effective torque was measured by preventing DNA rotation using a harmonic dihedral angle potential. The all-atom data are from Fig. 2c.$



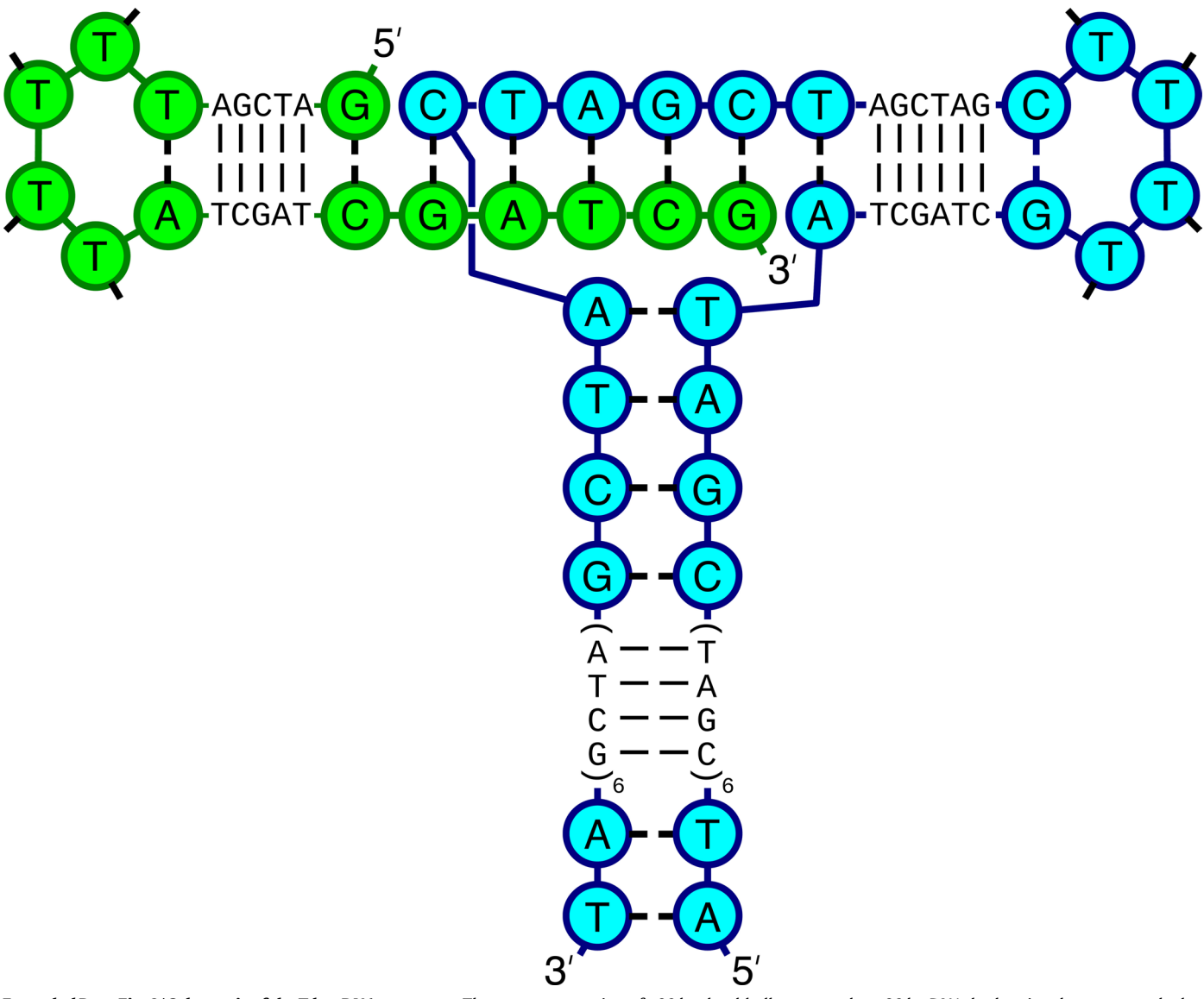
Extended Data Fig. 7 | **Water flow-induced rotation of a DNA molecule. a**, Simulation system containing a 21 bp DNA helix (light grey; green backbone) submerged in a volume of 1 M KCl electrolyte (semi-transparent molecular surface); only a fraction of ions is shown explicitly, for clarity. The DNA molecule is made effectively infinite by connecting each of its strands to itself over the periodic boundary of the simulation unit cell. For illustration, partial periodic images of the DNA molecule are shown in grey. The water flow is produced by applying a small, constant force to each water molecule parallel to the axis of the DNA molecule (see Methods). Phosphorus atoms of the DNA are harmonically restrained to the surface of a cylinder such that the DNA is free to rotate about

its axis; additional restrains prevent the molecules from drifting in the direction of the flow. **b**, Angular displacement of the DNA molecule as a function of simulation time. The sign of displacement is prescribed by the right-hand rule with respect to the positive direction of the force applied to the water molecules, as indicated in panel a. **c**, Average angular velocity of the DNA helix versus pressure gradient due to force applied to each water molecule. Each data point was determined by averaging a -60-200 ns MD trajectory. The line shows a linear regression fit to the data. The right axis displays the rotational velocity of the DNA in units of revolutions per minute (RPM).

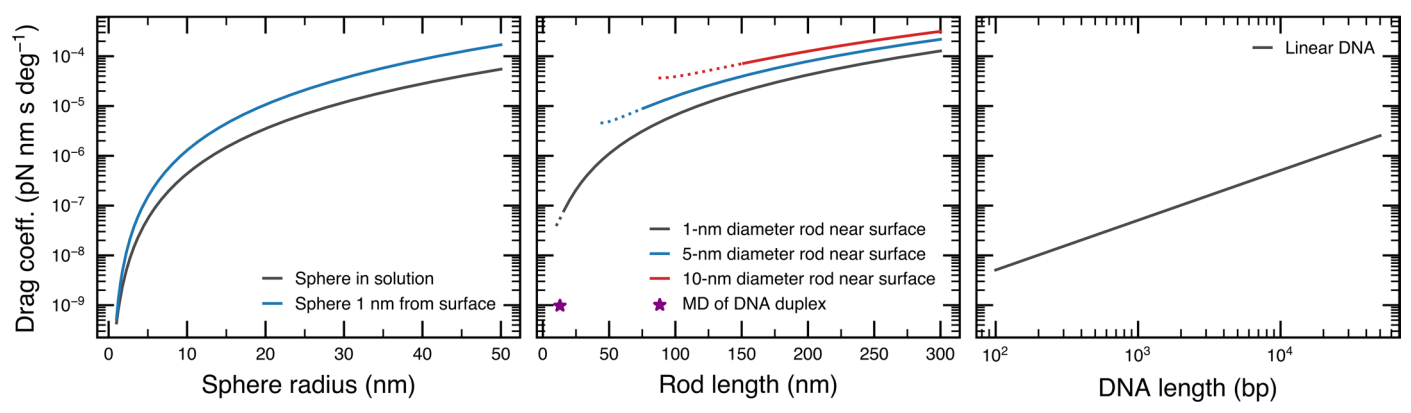


Extended Data Fig. 8 | Stochastic displacement of DNA pressed against a graphene surface. a, Side view of a simulation system consisting of a DNA duplex placed in contact with a layer of carbon atoms and 1 M KCl electrolyte solution, which is not shown for clarity. A 10 pN force is applied to the DNA centre of mass (CoM), pushing it towards the graphene. b, Sequence of snapshots illustrating spontaneous displacement of DNA along the graphene surface during a 150 ns MD simulation. A trace of the DNA CoM position is shown alongside the DNA (red to blue line). c, Mean squared displacement (MSD) of the CoM position of the DNA duplex. The CoM was projected into the plane of the graphene for MSD

calculation. Dashed line depicts a linear regression fit to the data. The effective diffusion coefficient of the DNA was extracted from the slope of the fit as $\langle \Delta x^2 \rangle = 4D\Delta t$. The diffusion coefficient was converted into a friction coefficient as $\gamma = k_B T/D$. **d**, MSD of the rotation angle of the DNA duplex. The rotation angle was obtained after projecting the duplex axis vectors into the plane of the graphene. The effective rotational diffusion coefficient was extracted from the slope of the fit as $\langle \Delta \theta^2 \rangle = 2D_{\rm rot} \Delta t$. The rotational diffusion coefficient was converted into a rotational friction coefficient as $\gamma_{\rm rot} = k_B T/D_{\rm rot}$



 $\textbf{Extended Data Fig. 9} | \textbf{Schematic of the T-bar DNA construct.} \ The construct consists of a 20 bp dumbbell connected to a 30 bp DNA duplex via a three-way stacked DNA junction. The two DNA strands are coloured in green and blue.$



Extended Data Fig. 10 | Scaling of the rotational friction coefficient with the size of the rotating object. Left, centre and right panels show theoretical dependences of the rotational drag coefficients of a sphere, of a rod and of a DNA molecule rotating about its axis, respectively. Theoretical expressions for the spherical and rod-like objects are provided in Methods. For a DNA load, the drag coefficient per basepair was taken to be 1.23 degrees $ns^{-1} pN^{-1} nm^{-1}$, a value

extracted from the all-atom MD simulations presented in Fig. 2d. The purple star in the middle panel depicts the friction coefficient extracted from our all-atom MD simulation of a DNA duplex pressed against a graphene surface (see Extended Data Fig. 7 for details) after accounting for the difference between the simulated and experimental viscosity values.